Atmos. Meas. Tech. Discuss., doi:10.5194/amt-2016-319, 2016
Manuscript under review for journal Atmos. Meas. Tech.
Published: 10 October 2016

Atmospheric Measurement Techniques Discussions

Development of a portable Cavity Enhanced Absorption Spectrometer for the measurement of ambient N_2O_5: experimental setup, lab characterizations, and field applications under polluted urban environment

Haichao Wang[1], Jun Chen[2], Keding Lu[1]

[1]State Key Joint Laboratory of Environmental Simulation and Pollution Control, College of Environmental Sciences and Engineering, Peking University, Beijing, China

[2]Institute of Particle and Two-Phase Flow Measurement, College of Energy and Power Engineering, University of Shanghai for Science and Technology, Shanghai, China

Correspondence to: K. Lu (k.lu@pku.edu.cn)

Abstract. A small and portable incoherent broadband cavity enhanced absorption spectrometer (IBBCEAS) for the dinitrogen pentoxide (N_2O_5) measurement has been developed. The instrument is featured with a mechanically aligned nonadjustable optical mounting system. To minimize the influence of the aerosol extinction and strong nonlinear absorption by water vapor, a dynamic reference spectrum with NO titration is used for the spectrum analysis. The range of spectrum fitting is 640-680 nm. Moreover, the wall losses of NO_3 and N_2O_5 on the surface of the inlet and cavity tubes were extensively characterized. We determined that the surface reactivity for the heated PFA materials toward NO_3 and N_2O_5 is 0.16 s^{-1} ± 0.04 s^{-1} and 0.019s^{-1} ± 0.004 s^{-1}, respectively. The N_2O_5 transmission efficiencies over the filter is 93% (± 3%). For the typical field experimental set up we used, the total transmission efficiency is about 82.9%, the optimal limit of the detection (LOD) is estimated as 1.9 ppt (1σ) at 50 s intervals, the total uncertainty of the N_2O_5 measurement is 15%, which is dominated by the uncertainty of the NO_3 cross section calculated for 353K in this system. Our instrument has been successfully deployed in two comprehensive field campaigns conducted in northern rural areas of Beijing in 2016. In both campaigns, the new design of the optical mounting system enabled us a fast setup and stable running of the IBBCEAS system for the detection of N_2O_5. High concentrations of N_2O_5 up to 1 ppb were detected for the two campaigns indicating an active nighttime chemistry presented in rural Beijing.

1 Introduction

Dinitrogen pentoxide (N_2O_5) is one of the most important reactive nitrogen species which plays an central role on the nighttime radical chemistry through its fast exchange with the NO_3 radical; meanwhile, the heterogeneous uptake of N_2O_5 by ambient aerosols is one of the two most important removal pathways of NOx which affects the NOx budget from regional to global scale (Brown et al., 2012; Wang et al., 2015). In recent studies, uptake of N_2O_5 on the aerosols which contain chloride ions was found to produce considerable amount of $ClNO_2$ at night and show potential strong impact on the next day chemistry

Atmos. Meas. Tech. Discuss., doi:10.5194/amt-2016-319, 2016
Manuscript under review for journal Atmos. Meas. Tech.
Published: 10 October 2016

Atmospheric Measurement Techniques Discussions

through the production of Cl radical by the photolysis of $ClNO_2$ (Osthoff et al., 2008; Thornton et al., 2010). In the study of the N_2O_5 chemistry, the quantification and the detailed mechanism of the N_2O_5 uptake processes is the major gap to be filled in the future studies. However, the high NOx and high aerosol regions is the most suitable condition to carry on the study. As the satellite data showed, the US, Europe and China are the three major NOx regions (i.e. Richter et al., 2005) while the North China Plain is the only one overlap with high aerosol loadings. Since extensively field studies of N_2O_5 were conducted in US and Europe (i.e. Brown et al., 2006; Crowley et al., 2010; Benton et al., 2010), direct observations of N_2O_5 for Chinese mega-city regions are of high value for the further exploration of the N_2O_5 chemistry.

There are a few existing optical spectroscopy and mass spectrometry methods for the detection of N_2O_5 such as cavity ring-down spectroscopy (CRDS), cavity enhance absorption spectroscopy (CEAS), laser-induced fluorescence (LIF), and chemical ionization mass spectrometry (CIMS). With respect to CIMS, there are two possible methods utilizing different ionization reactions with different target ions like NO_3^- (Slusher et al., 2004) and $I(N_2O_5)^-$ (Kercher et al., 2009). The method with NO_3^- is susceptible to chemical interference like $ClONO_2$, $BrONO_2$ (Chang et al., 2011) and was found to have strong interference under high NOx regime in Hongkong (Wang et al., 2014). The method with $I(N_2O_5)^-$ is better and showed good comparison versus a well-established CRDS system (Kercher et al., 2009; Wang et al., 2016). With respect to the optical approaches, a thermal decomposition plus a subsequent detection of the generated NO_3 radicals based on its absorption features in the visible spectral regions is required. (Yokelson et al., 1994). CRDS is the first technique used in the field measurement by detecting the N_2O_5 via its thermal conversion to NO_3 (Simpson et al., 2001), which has high temporal and spatial resolution with high sensitivity and accuracy (Brown et al., 2002; Dube et al., 2006). In the comparison the temporal resolution and sensitivity of LIF is relatively low due to the low fluorescence quantum yield of NO_3 and is subject to interferences from NO_2 in the high NOx region (Matsumoto et al., 2005). According to intercomparison experiments under simulated conditions (Fuchs et al., 2012), the IBBCEAS technique (Fiedler et al., 2003; Ball et al., 2004; Langridge et al., 2006; Venables et al., 2006; Langridge et al., 2008; Benton et al., 2010; Kennedy et al., 2011) showed similar detection capability of N_2O_5 to the CRDS system. Both CEAS and CRDS systems applied optical cavity, the CEAS measure the absorption spectrum of a wavelength window while the CRDS observed cavity decay time caused by the molecules at specific wavelength. Therefore, the CEAS shows a better selectivity while the CRDS shows a better sensitivity.

The measurement of N_2O_5 is still sparse in mainland China. The only published work was a field study performed at a mountain site in Hongkong (Wang et al., 2016; Brown et al. 2016), of which high N_2O_5 concentrations up to 8 ppbv were observed with two systems based on CIMS and CRDS, respectively. By considering the chemical complex environment presented in the Chinese City Clusters and the high NOx emissions, we think the selectivity may be more important. In addition, to probe the nighttime chemistry, vertical profile measurement is more important than the study of the daytime chemistry since the ambient air is highly stratified at night (Stutz et al., 2004). Thus, a portable IBBCEAS system to detect ambient N_2O_5 concentrations was developed to carry out the study. This system is distinct from previous

Atmos. Meas. Tech. Discuss., doi:10.5194/amt-2016-319, 2016
Manuscript under review for journal Atmos. Meas. Tech.
Published: 10 October 2016

N_2O_5-BBCEAS systems (Langridge et al., 2008; Kennedy et al.,2011) of its rigid cavity design and the usage of a dynamic zero point calibration system. This newly built instrument was deployed in two recent campaigns performed at two rural sites in Beijing. In this work, the detailed setup of our instrument, lab characterizations and its first field measurement results will be presented.

2 Instrument description

2.1 The Incoherent Broad Band Cavity Enhanced Absorption Spectroscopy

IBBCEAS, proposed by Fiedler et al. (2003), is a cavity-enhanced method which comprises a broad band light source, a high finesse optical cavity with high reflectivity mirrors, and a spectrograph with a CCD camera. The IBBCEAS technique in general combines the simplicity in the experimental setup, a high selectivity as the LP-DOAS method due broad spectra band and a high sensitivity with the long effective path length. This technique has been successfully utilized to measure a number of atmospheric trace gas compounds like HONO, H_2O, IO, O_3, O_4, I_2, IO, OIO, SO_2, NO_3, N_2O_5, glyoxal (CHOCHO) and methylgloxal (CH_3COCHO) (Washenfelder et al., 2008; Thalman and Volkamer, 2010; Gherman et al., 2008; Axson et al., 2011; Kahan et al., 2012; Washenfelder et al., 2013; Washenfelder et al., 2016; Min et al., 2016). The detection of NO_3 with this technique had been shown to be successful in the simulation chamber conditions with open-path IBBCEAS setup (Venables et al. 2006; Varma et al., 2009). Shortly afterwards, the closed cavity type of IBBCEAS was set up and shown to be successful in a surface measurement of NO_3+N_2O_5 (Langridge et al. 2008; Benton et al., 2010) and in a flight measurement of NO_3 and N_2O_5 (Kennedy et al. 2011).

The principle of IBBCEAS system in this work is similar as previous ones listed above and only introduced briefly here. The extinction coefficient, α, in the cavity can be described as Eq. 1 for the weak absorptions. On the one hand, α can be deduced by the measureable terms such as light transmission through the cavity, the mirror reflectivity and the effective cavity length; on the other hand, α is intrinsically caused by the absorption of the sample gases, the Rayleigh scattering of the sample gases and the Mie scattering of the aerosol from the sample gas.

$$\alpha(\lambda) = \left(\frac{I_0(\lambda)}{I(\lambda)} - 1\right)\left(\frac{1 - R(\lambda)}{d_{eff}}\right) = \sum_i n_i \sigma_i + \alpha_{mie} + \alpha_{rayl} \qquad \text{(Eq.1)}$$

Of Eq. 1, λ is the wavelength of light, n_i and $\sigma_i(\lambda)$ are the number density and absorption cross section of the i_{th} gas compound which causes absorption of the incidental light, d_{eff} is the effective cavity length, $R(\lambda)$ is the mirror reflectivity, $\alpha_{Ray}(\lambda)$ is the extinction due to Rayleigh scattering and $\alpha_{Mie}(\lambda)$ is the extinction due to Mie scattering, $I_0(\lambda)$ is the reference spectrum, and $I(\lambda)$ is the measured spectrum.

A least square spectral fitting method based on the IDL (Interface Define Language) is developed for retrieving molecule number densities of the species, the targets are the molecule number densities of NO_3 and NO_2, the molecule number densities of NO_2 is in sample of ambient air after thermal decomposed which is not exactly the same as ambient concentration. Spectra fitting window is from 640 to 680 nm, and a three-order polynomial was applied to fit the drift of light intensity and other scattering effect.

Atmos. Meas. Tech. Discuss., doi:10.5194/amt-2016-319, 2016
Manuscript under review for journal Atmos. Meas. Tech.
Published: 10 October 2016

2.2 Optical layout

The instrument schematic layout is shown in Fig.1. The system comprises several parts: a temperature stabilized light source, an optical cavity fixed on the aluminum profile and a commercial spectrograph with CCD detector. A single light emitting diode (LZ1-00R200, LedEngin, Marblehead, MA, USA) was used as a light source. It provided 1000 mW nominal optical power centered at deep red light region (662 nm) and the full width at half maximum (FWHM) is 25 nm when the LED temperature is stabilized at 17.5±0.1 °C to minimize the emission spectral shift by using a heat sink with thermo-electric cooler (TEC) control module . The LED is also mounted on a 3 dimension (3D) adjustable bracket which can be adjusted to improve the cavity alignment.

The optical cavity designed to be pressure and temperature insensitive. Therefore high reflectivity cavity mirrors are mechanically aligned with high precision mirror mounting parts based on pilot experiments. In the pilot experiments, the distances and positions of different mirrors/lens are tested and optimized to achieve maximum light output of the cavity. The advantage of this mirror mounting design is the high stability and fast setup of the cavity system for the purpose of the field measurements. The disadvantage is that one mirror mounting system is only suited best for specific type (wavelength region, thickness and curvature et al.) of cavity mirrors. In the current setup, the optical cavity consists of a pair of high reflective (HR) mirrors. The peak reflectivity of the mirrors at 660 nm is of about 0.999936 with the radii of curvature of 100 ± 5 cm (Layertec GmbH, Mellingen, Germany), the diameter of the mirrors is 25.0 (−0.1) mm. The two mirrors is mounted on two opposite located customized lens tubes, which are separated by 50.0 cm. Each HR mirror is continuously purged by 100 ml/min pure nitrogen flow to prevent the particle pollution enrolled by the sample gas flow. The optical cavity is enclosed by a sample gas flow tube and two corrugated pipes. The ambient air is sampled through an aerosol filter into the flow tube so that the aerosol extinction can be reduced significantly. This design is especially important for the use of such system for high aerosol loading environment. The corrugated pipes are used to buffer the length change of the sample flow tube under heated conditions. The light source and the optical components are homocentric integrated on an aluminum profile (75 × 8 × 5 cm). A 30 mm focal length achromatic lens is installed the lens tube 1 (L1) near the light source side as collimating lens. On the other side of the cavity, a 50 mm focal length achromatic lens is installed in the lens tube 2(L2) after the cavity HR mirror which further coupling the transmitted light onto a 100 μm diameter, 0.22 numerical aperture optical fiber. The fiber is mounted on a 3D adjustable bracket to improve the fiber coupling through relative movement toward the 50 mm lens. Finally, the fiber directed the cavity output light into the Ocean Optics QE65000 spectrometer (Dunedin, FL, USA). The charged couple device (CCD) in the QE65000 spectrograph is thermally regulated at −20.0 °C to minimize dark current. The line density of diffraction grating of the spectrometer is 1200 mm^{-1}, the entrance slits width is 100 μm and the spectral resolution FWHM is 0.85 nm with the wavelength coverage 580-710 nm. The instrument is working under the SNR (Signal Noise Ratio) estimation larger than 500:1.

2.2 Flow system

The instrument sample flow system included the inlet tube, aerosol filter, thermal dissociation module and heated sample flow tube, purge flow, mirror reflectivity calibration module, NO titration module and

Atmos. Meas. Tech. Discuss., doi:10.5194/amt-2016-319, 2016
Manuscript under review for journal Atmos. Meas. Tech.
Published: 10 October 2016

air mass sensors (T, P and RH).

The sample gas flow tube is made by a 35.6 cm long perfluoroalkoxy polymerresin (PFA) coated stand steel tube, the inner diameter (ID) is 10.0 mm. One end of the cavity connected a PFA inlet interface and the other end connected the outlet interface, the inlet/outlet interface is 1.8 cm long and the ID is also 10.0 mm, the distance between the inlet and outlet is 37.4 cm, but the total length of the PFA inner coated is 39.2 cm. With this combination, the loss of NO_3 during detection is minimized.

A Teflon polytetrafluoroethylene (PTFE) membrane filter (25 μm thickness, 4.6 cm diameter, 2.5 μm pore size) is used to remove ambient aerosol and protect the HR mirrors. A 35 cm long 1/4 inch ID PFA tube is installed between the filter and the inlet interface. This preheater tube is heated and stabilized at 120 °C serving as a thermal dissociation reactor for N_2O_5. When the sample flow rate is 2.0 L/min, the residence time in the thermal dissociation tube is about 0.13 s. With this setup of temperature and residence time, N_2O_5 will be completely decomposed to NO_3 in front of the preheater tube. The sample gas flow tube is heated and stabilized to 80 °C to prohibit the reversed reaction of NO_3 and NO_2 into N_2O_5. Between the filter and the thermal dissociation chamber, the NO titration module is inserted by a tee-piece PFA to add the NO gas. Details of the NO titration module will be given in Sect. 3.4. The mirror reflectivity calibration is done by calculation the difference of the Rayleigh extinction coefficient between pure N_2 and He gases (Washenfelder et al., 2016; Min et al., 2016). For our system, the calibration gases are introduced into the cavity through the mirror purge flow lines.

3 Characterization of the instrument key parameters

According to the Eq.1, there are several key parameters can affect the precision and accuracy of the measurement including: the cross section of the target species, effective cavity length, mirror reflectivity and reference spectrum.

3.1 The absorption cross section ($\sigma_i(\lambda)$)

To retrieve molecule number densities from the Eq. (1), the effective absorption cross section of the abundant ambient absorbers is necessary in this wavelength window such as NO_3, NO_2 and H_2O. However, the H_2O molecule vibration and rotation line-strength for a moderate spectrograph to resolve and in variable humidity conditions is still a challenge task, in this work to bypass this problem by using a reference spectrum which contains the same amount of H_2O as the measurement spectrum. This is achieved by using NO titration for the setup of the reference spectrum (details see Sect. 3.4). Therefore this method enables a fast data processing during a field campaign which could be benefit for providing online measurement readings.

The NO_3 absorption cross section is known as temperature dependent (Wangberg et al., 1997; Sander, 1986; Ravishankara and Mauldin, 1986; Yokelson et al., 1994; Orphal et al., 2003; Osthoff et al., 2007). The NO_3 absorption cross section at standard condition is referred to Yokelson et al. (1994). For the heated cavity conditions (353K), the cross section of the NO_3 were calculated by two steps: first, scaling the NO_3 cross section profile from Yokelson et al. (1994) to the band's peak intensity at 662 nm at 353 K from Osthoff et al. (2007); secondly, determining the instrument absorption cross section by convolving

Atmos. Meas. Tech. Discuss., doi:10.5194/amt-2016-319, 2016
Manuscript under review for journal Atmos. Meas. Tech.
Published: 10 October 2016

the scaled cross section with an instrument function (taken from the neon emission line at 659.48nm). Fig.2 is the result of the scaled and convolved NO_3 absorption cross section at 353 K and the convolved NO_2 absorption cross section. The absorption cross section of NO_3 near the 662 nm at 353K is three orders of magnitude larger than that of NO_2 while the ambient N_2O_5 concentration is normally two orders of magnitude smaller than that of NO_2 during nighttime, so the cavity detected NO_3 absorption near 662 nm will dominate the total absorption at night.

3.2 The effective cavity length (d_{eff})

The experimental determination of the total extinction coefficient requires the knowledge on the effective cavity length d_{eff}, which represented the cavity length occupied by the absorbing gas sample when the sampling flow is stable. Since the continuously purge flow occupied the two ends of the cavity to protect the mirrors, the d_{eff} usually shorter than the distance between the two high reflective mirrors and longer than the distance between the sampling inlet and outlet. We determined the d_{eff} to be 45.0 cm for our cavity setup with standard gas of NO_2. The determined d_{eff} is larger than the length of the PFA coated part with 39.2 cm. Since the wall reactivity of NO_3 toward none PFA coated material could be quite large, we estimated the d_{eff} for NO_3 detection in our system to be 39.2 cm. different d_{eff} numbers were determined for NO_2 and NO_3, our solution is to apply the d_{eff} of NO_3 in Eg. (1) by adding a correction factor on the used NO_2 absorption cross section.

3.3 The mirror reflectivity ($R(\lambda)$)

The mirror reflectivity ($R(\lambda)$) is an important parameter to be determined in this instrument. In previous work, $R(\lambda)$ had been determined through the detection of stable trace gas compound with known concentrations (Venables et al., 2006), the differentiation of pure gases with distinct Rayleigh Scattering cross section (Chen and Venables, 2011; Washenfelder et al., 2016; Min et al., 2016), the use of low loss optics (Varma et al., 2009) and phase shift method (Langridge et al., 2008; Kennedy et al. 2011). In this study, measuring the pure N_2 and He Rayleigh scattering signals in the cavity through Eq. (2) is used to determine $R(\lambda)$ during field campaigns. The Rayleigh scattering cross sections for N_2 ($\alpha_{Ray,N2}(\lambda)$) and He ($\alpha_{Ray,He}(\lambda)$) are referred to Sneep and Ubachs (2005) and Shardanand and Rao (1977), respectively.

$$R(\lambda) = 1 - d\left(\frac{I_{N_2}(\lambda)n_{N_2}\sigma_{Rayl,N_2}(\lambda) - I_{He}(\lambda)n_{He}\sigma_{Rayl,He}(\lambda)}{I_{He}(\lambda) - I_{N_2}(\lambda)}\right) \qquad \text{(Eq. 2)}$$

Of Eq. (2), d is the distance between the two high reflective mirrors, $I_{N2}(\lambda)$ and $I_{He}(\lambda)$ represent the N_2 and He spectrum respectively, which were acquired by stopping the sampling flow and filling the N_2 or He with the cavity though the purge flow, n_{N2} and n_{He} are the number density of N_2 and He calculated by the measured the temperature and pressure in the cavity.

The Fig.3 shows the mirror reflectivity calculation result from the University of Chinese Academy of Science (UCAS) international field winter campaign, 2016. The bold black line is the averaged reflectivity of the five measurement of $R(\lambda)$, noted that the peak of the $R(\lambda)$ is 0.999936 ± 0.000002 at 662 nm. Under the protection of the purge flow and due to the rigid setup of the cavity system, the $R(\lambda)$ was

Atmos. Meas. Tech. Discuss., doi:10.5194/amt-2016-319, 2016
Manuscript under review for journal Atmos. Meas. Tech.
Published: 10 October 2016

remarkably stable during the field campaign. The bold red line is the averaged cavity loss, which is equal to the $(1-R(\lambda))/d$, the maximized point near 662 nm is $(1.28 \pm 0.01) \times 10^{-6}$ (1σ). The effective path length calculated at 662 nm is 6.13 km.

3.4 The reference spectrum ($I_0(\lambda)$)

In this work, two kinds of reference spectrum $I_0(\lambda)$ are recorded for the analysis of the ambient dataset. One reference spectrum is obtained by measuring pure N_2 gases; the other is obtained by adding NO into the ambient sample flow. When the reference spectrum with pure N_2 is applied to Eq. (1), we can retrieve NO_2, NO_3, and H_2O concentrations in the targeted wavelength window. Nevertheless, the absorption of the water vapor near 662 nm is a typical non-Beer–Lambert absorption, its absorption lines in the 4ν+δ polyad have pressure broadened half widths, which is much smaller than the resolution of spectrograph used in this work, so the effective cross section need to calculated frequently. Although there are several ways to fitting the water vapor absorption very well in the measurement as demonstrated in previous publications (Ravi et al., 2009; Langridge et al., 2008; Kennedy et al. 2011), fitting the water vapor absorption is not the purpose of this instrument. When the reference spectrum with NO addition is applied to Eq. (1), the calculated extinction spectrum would be quite clean of which only contain the positive absorption of NO_3 and negative absorption of NO_2. The same concept has been used by the CRDs for the detection of NO_3 and N_2O_5 (Brown et al., 2002). In current setup, the NO addition is modulated by a computer controlled solenoid valve, the flow of 98 ppm NO mixture in the N_2 is added with 10ml/min by a Teflon tube (O.D. = 1/4 inch), the excess NO is enough to chemical destructed the decomposing produced NO_3 completely during the 0.13 s residence time in the preheater tube, a dry N_2 line is added at the exit end of the solenoid valve by a PFA tee-piece to promote the diffusion of the residual NO at the beginning of the NO off-mode, as shown in the Fig. 4, the 1/8 inch OD Teflon tube of the N_2 flow inserted into the 1/4 inch OD Teflon tube in a contrary direction with a continuous small flow rate (10ml/min), in a typical measurement cycle of 5 min, NO is added into the sample flow for 20 s with 5s spectra integral time so that a kind of dynamic zero point can be used for the N_2O_5 detection. An example of the time series of ambient N_2O_5 detection for half an hour is shown as Fig. 5. The red points mark the effective ambient measurement result, which covered 4 minutes 20 s in every 5 minutes, the blue points include the 20 s background points and the 20 s ambient measurement points affected by the residual NO in the tube.

4 Result and discussion

4.1 Spectrum fitting

Fig. 6 shows an example of NO_3 spectrum fitting of an ambient measurement result at 5s. By using the reference spectrum given by the NO titration scheme described in Sect. 3.4, the fitting of NO_3 spectra is therefore a straight forward procedure. For most of the cases, NO_3 is the only target species during spectra process. Within the fitting window 640–680 nm, the fitted line in the Fig. 6a is corresponding to 74 ppt of N_2O_5 and the fitted line in the Fig. 6b represents 25ppt N_2O_5 in the cavity, the residuals of fitting for both cases are shown as the Fig. 6c. The fitting spectrum residual is in the range of $\pm$ 4.0x10^{-9}

Atmos. Meas. Tech. Discuss., doi:10.5194/amt-2016-319, 2016
Manuscript under review for journal Atmos. Meas. Tech.
Published: 10 October 2016

Atmospheric Measurement Techniques Discussions

cm^{-1} and absorption structure of NO_2 and H_2O is not observed in the residual spectrum.

4.2 Transmission efficiency of N_2O_5

For the accurate measurement of N_2O_5, the N_2O_5 wall loss in the sampling manifold and the NO_3 wall loss in the preheater and cavity need to be determined. To quantify those two loss processes, we defined two transmission factors of N_2O_5 correspondingly. Transmission factor 1 (T1) characterize the survived part of N_2O_5 from the inlet to the beginning of the preheater, which caused by the wall loss on the sampling tube and the filter loss on the filter holder, transmission factor 2 (T2) characterize the survived part of the produced NO_3 from N_2O_5 from the beginning of the preheater to the center of the cavity outlet. To determine these two factors, a N_2O_5 source is set up through a 160 L flow reactor. The known amount of gases of NO_2 and O_3 are generated by a gas calibrator (Thermo146i) and then delivered into flow reactor. Stable steady state concentration (±2%) of N_2O_5 can be built up after passing this reactor. Through modulate the ratio of supplied NO_2 and O_3; the ratio of N_2O_5 to NO_3 can be typically controlled to more than 100:1.

4.2.1 Wall loss of N_2O_5 in the sampling manifold

Two losses processes contributed to the determination of T1, one is the loss of N_2O_5 on the particle filter and the other is that on the inlet tubes. Following Brown et al. (2002), we attached a three-way Teflon valve at the inlet and the standard N_2O_5 gas flow is switched between two sample lines with and without a clean particle filter. Differentiation of the above two N_2O_5 measurement results determines the transmission efficiency through particle filter which is 93.0% for our typical instrument parameters, the frequent filter changing keeps the correction factors with small uncertainty (± 3%), which is similar to previous results (Brown et al., 2002; Fuchs et al., 2008).

To test the wall loss of the N_2O_5 in the PFA line, different lengths (0.5, 3.5, 5.5, 7.5, 10.5 m) of PFA tube (O.D. =1/4 inch) is inserted between the outlet of the reactor and the inlet of the preheater. The apparent first order loss rate of N_2O_5 (0.015 s^{-1}) is deduced by a linear fit of the observed N_2O_5 concentrations toward different the residence times corresponding to certain length of tubes (Fig. 6). The actual situation is more complicated in these sample lines that contains a series of reactions (R1-R5). And therefore the wall loss rate of N_2O_5 is further abstracted from the observed decay rate with a box model including R1-R5. In this model, initial NO_2 and O_3 are observed values at the outlet of the reactor; wall loss rate of NO_3 (R3) is set to be 0.16 s^{-1}, which was determined by another experiment explained later. The retrieved net N_2O_5 loss rate coefficient was 0.019 s^{-1} ± 0.004 s^{-1}, this result is smaller than the measured upper limit result 0.042 s^{-1} ± 0.003 s^{-1} by Kennedy et al. (2011). The typical 1.5 meter length of inlet sampling tube have the N_2O_5 transmission efficient at 98.9%. Transmission factor 1, T1, is therefore calculated to be 90.0% (±3.0 %) for the typical condition.

$N_2O_5 \rightarrow NO_3$ (R1)

N_2O_5 + wall → (R2)

NO_3 + wall → (R3)

Atmos. Meas. Tech. Discuss., doi:10.5194/amt-2016-319, 2016
Manuscript under review for journal Atmos. Meas. Tech.
Published: 10 October 2016

$NO_2 + O_3 \rightarrow NO_3$ (R4)

$NO_2 + NO_3 \rightarrow N_2O_5$ (R5)

4.2.2 Wall loss of NO_3 produced from N_2O_5 in the heated tubes

When the N_2O_5 goes into the preheater, wall loss of NO_3 produced from N_2O_5 thermal decomposition become the dominant contributor, which limited by the transmission factor 2. To determine the wall loss reactivity of NO_3, the optical cavity is used as a flow tube. Stable amount of N_2O_5 is built up in the optical cavity with a continuous flow mode. When stopping the flow, the observed NO_3 versus the elapsed time determines the first order loss rate of NO_3 ($0.22\ s^{-1} \pm 0.04\ s^{-1}$) in the optical cavity tube (see Fig. 8). The fitted first order uptake coefficient of NO_3 reflects the contribution from three processes: (1) the wall loss of the NO_3 in the cavity; (2) the dilution effect due to the purge flow in the cavity; (3) the production of NO_3 with available NO_2 and O_3. The third term is minimized by setting the NO_2 and O_3 concentrations to be small values (in our case, we used 35 ppb for both of them). The second term can be calculated according to the sample flow and purge flow rates, and it can be independently determined with the detection of NO_2 decay in the optical cavity after stopping the flow. With both methods, the dilution reactivity of our experimental setup determined to be $0.087 \pm 0.02 s^{-1}$. The wall loss reactivity of NO_3 is retrieved to be $0.16 \pm 0.04\ s^{-1}$ with a box model taking into account of the above three processes, which is in the range of the previous results with 0.1-0.3 s^{-1} (Brown et al.,2002; Crowley et al. 2010; Kennedy et al. 2011; Wang et al., 2015). Since the residence time in the preheater and cavity is 0.13 s and 0.83 s, the T_2 was calculated to be 92.1%. The total transmission efficiency of N_2O_5 (T_{N2O5}) can be calculated by $T_1 \times T_2$, was found to be 82.9%. Additionally, the total transmission efficiency of the ambient NO_3 (T_{NO3}) is calculated to be 63.6% when ignoring the NO_3 loss on the filter (Fuchs et al., 2008). These factors are suitable to be applied for the sampling by changing filter frequently.

4.3 Precision and uncertainty analysis

Fig. 9 shows the histogram of 5200 zero measurement results in the laboratory with 1 second time resolution, there exist an offset with -0.6 ppt and the limit of detection of 3.0 ppt (1σ). The limit of the detection and the stability of the instrument are further analyzed with Allan Variance method (Allan, 1966; Werle et al., 1993). Fig. 10 shows an Allan Variance analysis of the 12000 zero measurement spectrums in the laboratory with 1s integration time. According to the Allan deviation plot, the best limit of the detection is found to be 1.9 ppt (1σ) at 50 s intervals. The uncertainty of the instrument consists of the following parts: the uncertainty of the temperature corrected and convolved cross section of NO_3 is ± 13% from the same method of Kennedy et al. (2011); the effective cavity length calculation is ± 2%; the reflectivity determination uncertainty mainly controlled by the cross section of N_2 and He, which is about ± 5% together; the uncertainty of the transmission efficiency of the sampling and cavity system is about ± 3%, according to the Gaussian error propagation, the total uncertainty of N_2O_5 detection is estimated to be ± 15% in our system.

Atmos. Meas. Tech. Discuss., doi:10.5194/amt-2016-319, 2016
Manuscript under review for journal Atmos. Meas. Tech.
Published: 10 October 2016

Atmospheric Measurement Techniques Discussions

5 Instrument Performance in two comprehensive field campaigns

After the development and full characterization performed in the lab, our instrument had been successfully applied in two comprehensive field campaigns in 2016. The first campaign took place at the campus of University of Chinese Academy of Sciences (UCAS) from 6 January to 4 March while the second campaign took place at Peking University Changping campus from 15 May to 23 June 2016. As shown in Fig. 11, both sites are located in northern rural areas in Beijing, of about 60 km and 40 km to the center of Beijing city, respectively. According to our current understanding of the NO_3-N_2O_5 chemistry, rural areas are the transitional regions of the anthropogenic and biogenic emissions where high O_3 can meet with relatively high NO_2 so that the NO_3-N_2O_5 chemistry may be maximized. We expected these two sites to be ideal locations to probe the NO_3-N_2O_5 chemistry in Beijing.

During the UCAS campaign, our instrument was deployed at a roof lab and the sampling inlet was about 15 m above the ground. The measurement site is close to mountainous area in Beijing while influenced by nearby traffic emissions. When the northerly wind appeared, we sampled clean air masses entrained with local traffic and residential emissions; when southerly wind appeared, we could then capture the outflow of Beijing. In Figure 12(a), the observed N_2O_5 concentrations during a typical development of such air mass change from clean to polluted conditions are shown. It is worth to be noticed that the observed N_2O_5 also including the ambient signals from NO_3 as described in Eq. 3. Of Eq. 3, T_{NO3} is much smaller than T_{N2O5} as discussed in Sect. 4.2.2. Moreover, due to the conditions we experienced for the winter campaign, the ratio of N_2O_5/NO_3 is always larger than 10 so that this term $T_{NO3} \times C_{ambi}(NO_3)$ is ignored. For this reason, our detected N_2O_5 concentrations will have a positive bias less than 10%.

$$C_{obs}(N_2O_5) = T_{NO3} \times C_{ambi}(NO_3) + T_{N2O5} \times C_{ambi}(N_2O_5) \qquad \text{(Eq.3)}$$

High concentrations of N_2O_5 were observed at a near surface level at the UCAS site. As the development of the pollution episode, the maximum N_2O_5 concentrations even reached to be more than 1ppb in the night of Mar 02-03, 2016. Fast variation of N_2O_5 was also observed which might due to local traffic emissions during stagnant conditions. In all these days, the observed N_2O_5 continuous to accumulate in a few hours after sunset, reached its maximum before midnight and then gradually decreased to zero before sunrise. The decrease of the N_2O_5 concentrations at night in this location may be related to the typical running style of the heavy-duty vehicles (HDV). Typically, more heavy-duty cars were appeared on the nearby street after 22:00 since the ban of HDV entering into downtown Beijing is set to be after midnight. In addition, fast variation of the ambient N_2O_5 concentrations was captured indicating that the N_2O_5 distribution in the ambient air masses observed at UCAS was quite heterogeneous. This behavior has also been reported by many other field measurements (Brown et al., 2003; Slusher et al., 2004; Matsumoto et al., 2005; Ayers et al., 2006; Nikayama et al., 2007).

During the PKU-CP spring campaign, our instrument was set up on the fifth floor of the main building in PKU-CP campus. Our inlet was about 15 m above ground. During springtime in northern part of rural Beijing, high O_3 event would be presented (e.g. Wang et al., 2006). Together with the atmospheric

Atmos. Meas. Tech. Discuss., doi:10.5194/amt-2016-319, 2016
Manuscript under review for journal Atmos. Meas. Tech.
Published: 10 October 2016

processes with high NO_2 conditions, high NO_3 and N_2O_5 concentrations can be expected. At this location, a steady state calculation showed that the dominant ratio of N_2O_5/NO_3 was again larger than 10 so that our direction observations again showed that there were high N_2O_5 concentrations presented at evening hours (Figure 12(b)). During the campaign, an Aerodyne I⁻CIMS (Breton et al., 2012；Breton et al., 2014) was deployed in parallel with our instrument. A preliminary comparison showed that there were good agreements of the observed N_2O_5 between the two instruments. Details of this comparison will be presented in a future publication.

6 Conclusions

Detection of N_2O_5 is an attractive and challenge work to explore the atmospheric oxidation capacity and the NOx removal at night. N_2O_5 chemistry is very active and important for areas with the presence of high O_3 and high NO_2 as well as high aerosol loadings. The Chinese megacities are these kind of areas which fulfill such requirement and are expected to be the global hot spots of N_2O_5 chemistry. The cavity based absorption techniques (e.g. CRDS and CEAS) and CIMS are the available technical options for the field detection of N_2O_5.

In the present work, we developed a new portable N_2O_5 spectrometer featured with a mechanically aligned lens tubes for the setting up of HR mirrors. The new design offers us a fast setup of the instrument in the field and the instrument are proved to be running stably for a few months in two field campaigns. Except the new design of the HR mirror mounting parts, a few important engineering work is explored during setting up of the instrument. Temperature control of the light source (e.g. LED in our case) is of crucial importance for the subsequent spectrum analysis. The using of the corrugated pipes in between the mirror-mounting lens tubes and the cavity tube is critical to make the system to be stable for the heated conditions. Since the mirror-mounting lens tubes are mechanically fixed, three-dimensional adjustment of the light source and the fiber receiver is required to maximize the optical signal collected by the detector.

In the lab, this work systematically characterized the key parameters of our N_2O_5 spectrometer such as the mirror reflectivity and effective cavity length. The mirror reflectivity is found to be larger than 99.99% as stated by the producer and the determined results were variable within 2%, which again showed the advantage of this mechanically, aligned HR mirror-mounting lens tubes. A dynamic reference spectrum generated by adding NO into the sample flow is tested and proved to be very helpful for the ambient spectrum analysis that avoided the complicated fitting of H_2O absorption. The wall losses of the inlet system and the cavity tubes were also extensively characterized. The wall loss rate of the N_2O_5 in the sampling tube is determined to 0.019 s^{-1} ±0.004 s^{-1} and the wall loss rate of the NO_3 radical produced from thermally decomposed N_2O_5 in the preheater tube and the cavity tube is 0.16 s^{-1} ±0.04 s^{-1}, the transmission efficiency of N_2O_5 on the filter is 93(± 3)%, based on the mentioned parameters above, the total N_2O_5 loss on the surface of the filter and the total transmission efficiency is about 82.9%, the calibration factor used to calibrate the measured concentration to the ambient concentration is 1.20, and the total accuracy of the measurement is determined to be ± 15%. The best fitting wavelength window is

Atmos. Meas. Tech. Discuss., doi:10.5194/amt-2016-319, 2016
Manuscript under review for journal Atmos. Meas. Tech.
Published: 10 October 2016

found to be 640–680 nm, and the measurement precision is quantified to be 3.0 ppt (1σ) in 1 second and the Allan deviation analysis indicated that the best detection limit could be achieved as 1.9 ppt (1σ) at 50 s intervals.

Our N_2O_5 spectrometer had been successfully applied in the field measurements of N_2O_5 during the 2016 UCAS winter campaign (Jan - Mar) and the 2016 PKU-CP spring campaign (May - Jun). In the example time series we presented herein, high and highly variable concentrations of near surface N_2O_5 concentrations were detected for Beijing rural areas. These high near surface N_2O_5 concentrations indicating that there were very active nighttime NO_3-N_2O_5 chemistry as well as the daytime OH chemistry (Lu et al., 2013; Lu et al., 2014; Tan et al., 2016) in the North China Plain. In a recent source term diagnosis of the secondary organic aerosols, it is found that the nighttime NO_3 oxidation could even dominate the formation of organic nitrates over Europe (Kiendler-Scharr et al., 2016). Since all the Chinese megacity areas are the NOx hot spot worldwide, it will be therefore of crucial importance to bridge the daytime OH chemistry and the nighttime NO_3 chemistry in the near future in China. Our current developed portable N_2O_5 instrument and a planned portable NO_3 instrument can serve as the useful tool to explore the formation of the atmospheric oxidation capacity in such areas.

Atmos. Meas. Tech. Discuss., doi:10.5194/amt-2016-319, 2016
Manuscript under review for journal Atmos. Meas. Tech.
Published: 10 October 2016

Acknowledgements.

The work was supported by the National Natural Science Foundation of China (Grant No. 41375124，21522701, 21190052, 91544225), Strategic Priority Research Program of the Chinese Academy of Sciences (grant no. XDB05010500). The authors gratefully acknowledge the discussions and suggestions from Steven Brown, Kyung-Eun Min, Bin Ouyang, Ravi Varma, Hendrik Fuchs and Zhiguo Wu. We thank the team of the UCAS (organized by Yuanhang Zhang) and Changping Campaigns (organized by Min Hu and Mattias Hallquist).

References

Allan, D. W.: Statistics of Atomic Frequency Standards, Pr Inst Electr Elect, 54, 221-230, 1966.

Axson, J. L., Washenfelder, R. A., Kahan, T. F., Young, C. J., Vaida, V., and Brown, S. S.: Absolute ozone absorption cross section in the Huggins Chappuis minimum (350-470 nm) at 296 K, Atmos Chem Phys, 11, 11581-11590, 2011.

Ayers, J. D. and Simpson, W. R.: Measurements of N2O5 near Fairbanks, Alaska, J Geophys Res-Atmos, 111, 2006.

Ball, S. M., Langridge, J. M., and Jones, R. L.: Broadband cavity enhanced absorption spectroscopy using light emitting diodes, Chem Phys Lett, 398, 68-74, 2004.

Benton, A. K., Langridge, J. M., Ball, S. M., Bloss, W. J., Dall'Osto, M., Nemitz, E., Harrison, R. M., and Jones, R. L.: Night-time chemistry above London: measurements of NO3 and N2O5 from the BT Tower, Atmos Chem Phys, 10, 9781-9795, 2010.

Brown, S. S., Dube, W. P., Tham, Y. J., Zha, Q. Z., Xue, L. K., Poon, S., Wang, Z., Blake, D. R., Tsui, W., Parrish, D. D., and Wang, T.: Nighttime chemistry at a high altitude site above Hong Kong, J Geophys Res-Atmos, 121, 2457-2475, 2016.

Brown, S. S., Stark, H., Ciciora, S. J., McLaughlin, R. J., and Ravishankara, A. R.: Simultaneous in situ detection of atmospheric NO3 and N2O5 via cavity ring-down spectroscopy, Review of Scientific Instruments, 73, 3291-3301, 2002.

Brown, S. S., Stark, H., Ciciora, S. J., and Ravishankara, A. R.: In-situ measurement of atmospheric NO3 and N2O5 via cavity ring-down spectroscopy, Geophys Res Lett, 28, 3227-3230, 2001.

Brown, S. S., Stark, H., Ryerson, T. B., Williams, E. J., Nicks, D. K., Trainer, M., Fehsenfeld, F. C., and Ravishankara, A. R.: Nitrogen oxides in the nocturnal boundary layer: Simultaneous in situ measurements of NO3, N2O5, NO2, NO, and O-3, J Geophys Res-Atmos, 108, 2003.

Brown, S. S. and Stutz, J.: Nighttime radical observations and chemistry, Chem Soc Rev, 41, 6405-6447, 2012.

Chang, W. L., Bhave, P. V., Brown, S. S., Riemer, N., Stutz, J., and Dabdub, D.: Heterogeneous Atmospheric Chemistry, Ambient Measurements, and Model Calculations of N2O5: A Review, Aerosol Sci Tech, 45, 665-695, 2011.

Chen, J. and Venables, D. S.: A broadband optical cavity spectrometer for measuring weak near-ultraviolet absorption spectra of gases, Atmos Meas Tech, 4, 425-436, 2011.

Atmos. Meas. Tech. Discuss., doi:10.5194/amt-2016-319, 2016
Manuscript under review for journal Atmos. Meas. Tech.
Published: 10 October 2016

Crowley, J. N., Schuster, G., Pouvesle, N., Parchatka, U., Fischer, H., Bonn, B., Bingemer, H., and Lelieveld, J.: Nocturnal nitrogen oxides at a rural mountain-site in south-western Germany, Atmos Chem Phys, 10, 2795-2812, 2010.

Crowley, J. N., Schuster, G., Pouvesle, N., Parchatka, U., Fischer, H., Bonn, B., Bingemer, H., and Lelieveld, J.: Nocturnal nitrogen oxides at a rural mountain-site in south-western Germany, Atmos Chem Phys, 10, 2795-2812, 2010.

Dube, W. P., Brown, S. S., Osthoff, H. D., Nunley, M. R., Ciciora, S. J., Paris, M. W., McLaughlin, R. J., and Ravishankara, A. R.: Aircraft instrument for simultaneous, in situ measurement of NO3 and N2O5 via pulsed cavity ring-down spectroscopy, Review of Scientific Instruments, 77, 2006.

Fiedler, S. E., Hese, A., and Ruth, A. A.: Incoherent broad-band cavity-enhanced absorption spectroscopy, Chem Phys Lett, 371, 284-294, 2003.

Fuchs, H., Dube, W. P., Cicioira, S. J., and Brown, S. S.: Determination of inlet transmission and conversion efficiencies for in situ measurements of the nocturnal nitrogen oxides, NO3, N2O5 and NO2, via pulsed cavity ring-down spectroscopy, Analytical chemistry, 80, 6010-6017, 2008.

Fuchs, H., Simpson, W. R., Apodaca, R. L., Brauers, T., Cohen, R. C., Crowley, J. N., Dorn, H. P., Dube, W. P., Fry, J. L., Haseler, R., Kajii, Y., Kiendler-Scharr, A., Labazan, I., Matsumoto, J., Mentel, T. F., Nakashima, Y., Rohrer, F., Rollins, A. W., Schuster, G., Tillmann, R., Wahner, A., Wooldridge, P. J., and Brown, S. S.: Comparison of N2O5 mixing ratios during NO3Comp 2007 in SAPHIR, Atmos Meas Tech, 5, 2763-2777, 2012.

Gherman, T., Venables, D. S., Vaughan, S., Orphal, J., and Ruth, A. A.: Incoherent broadband cavity-enhanced absorption spectroscopy in the near-ultraviolet: Application to HONO and NO2, Environ Sci Technol, 42, 890-895, 2008.

Kahan, T. F., Washenfelder, R. A., Vaida, V., and Brown, S. S.: Cavity-Enhanced Measurements of Hydrogen Peroxide Absorption Cross Sections from 353 to 410 nm, Journal of Physical Chemistry A, 116, 5941-5947, 2012.

Kennedy, O. J., Ouyang, B., Langridge, J. M., Daniels, M. J. S., Bauguitte, S., Freshwater, R., McLeod, M. W., Ironmonger, C., Sendall, J., Norris, O., Nightingale, R., Ball, S. M., and Jones, R. L.: An aircraft based three channel broadband cavity enhanced absorption spectrometer for simultaneous measurements of NO3, N2O5 and NO2, Atmos Meas Tech, 4, 1759-1776, 2011.

Kercher, J. P., Riedel, T. P., and Thornton, J. A.: Chlorine activation by N2O5: simultaneous, in situ detection of ClNO2 and N2O5 by chemical ionization mass spectrometry, Atmos Meas Tech, 2, 193-204, 2009.

Kiendler-Scharr, A., Mensah A. A., Friese, E., Topping, D. Nemitz, E., Prevot, A. S. H., ÄijäläMensah, M., Allan, J., Canonaco, F., Canagaratna, M., Carbone, S., Crippa, M., Dall Osto, M., Day, D. A., De Carlo, P., Di Marco, C. F., Elbern, H., Eriksson, A., Freney, E., Hao, L., Herrmann, H., Hildebrandt, L., Hillamo, R., Jimenez, J. L., Laaksonen, A., McFiggans, G., Mohr, C., O'Dowd, C., Otjes, R., Ovadnevaite, J., Pandis, S. N., Poulain, L., Schlag1, P., Sellegri, K., Swietlicki, E., Tiitta, P., Vermeulen, A., Wahner, A., Worsnop, D., and Wu, H. C.: Ubiquity of organic nitrates from nighttime chemistry in the European submicron aerosol, Geophys Res Lett, 43, 2016.

Kraus, S. G.: DOASIS: A Framework Design for DOAS, Dissertation, University of Mannheim, Mannheim, Germany, 2006.

Langridge, J. M., Ball, S. M., and Jones, R. L.: A compact broadband cavity enhanced absorption spectrometer for detection of atmospheric NO2 using light emitting diodes, Analyst, 131, 916-922, 2006.

Langridge, J. M., Laurila, T., Watt, R. S., Jones, R. L., Kaminski, C. F., and Hult, J.: Cavity enhanced absorption spectroscopy of multiple trace gas species using a supercontinuum radiation source, Opt Express, 16, 10178-10188, 2008.

Le Breton, M., Bacak, A., Muller, J. B. A., Bannan, T. J., Kennedy, O., Ouyang, B., Xiao, P., Bauguitte, S. J. B., Shallcross, D. E., Jones, R. L., Daniels, M. J. S., Ball, S. M., and Percival, C. J.: The first airborne comparison of N2O5 measurements over the UK using a CIMS and BBCEAS during the RONOCO campaign, Anal Methods-Uk, 6, 9731-9743, 2014.

Le Breton, M., McGillen, M. R., Muller, J. B. A., Bacak, A., Shallcross, D. E., Xiao, P., Huey, L. G., Tanner, D., Coe, H., and Percival, C. J.: Airborne observations of formic acid using a chemical ionization mass spectrometer, Atmos Meas Tech, 5, 3029-3039, 2012.

Lu, K. D., Hofzumahaus, A., Holland, F., Bohn, B., Brauers, T., Fuchs, H., Hu, M., Haseler, R., Kita, K., Kondo, Y., Li, X., Lou, S. R., Oebel, A., Shao, M., Zeng, L. M., Wahner, A., Zhu, T., Zhang, Y. H., and Rohrer, F.: Missing OH source in a suburban environment near Beijing: observed and modelled OH and HO2 concentrations in summer 2006, Atmos Chem Phys, 13, 1057-1080, 2013.

Lu, K. D., Rohrer, F., Holland, F., Fuchs, H., Brauers, T., Oebel, A., Dlugi, R., Hu, M., Li, X., Lou, S. R., Shao, M., Zhu, T., Wahner, A., Zhang, Y. H., and Hofzumahaus, A.: Nighttime observation and chemistry of HOx in the Pearl River Delta and Beijing in summer 2006, Atmos Chem Phys, 14, 4979-4999, 2014.

Matsumoto, J., Kosugi, N., Imai, H., and Kajii, Y.: Development of a measurement system for nitrate radical and dinitrogen pentoxide using a thermal conversion/laser-induced fluorescence technique, Review of Scientific Instruments, 76, 2005.

Min, K. E., Washenfelder, R. A., Dube, W. P., Langford, A. O., Edwards, P. M., Zarzana, K. J., Stutz, J., Lu, K., Rohrer, F., Zhang, Y., and Brown, S. S.: A broadband cavity enhanced absorption spectrometer for aircraft measurements of glyoxal, methylglyoxal, nitrous acid, nitrogen dioxide, and water vapor, Atmos Meas Tech, 9, 423-440, 2016.

Nakayama, T., Ide, T., Taketani, F., Kawai, M., Takahashi, K., and Matsumi, Y.: Nighttime measurements of ambient N2O5, NO2, NO and O-3 in a sub-urban area, Toyokawa, Japan, Atmos Environ, 42, 1995-2006, 2008.

Orphal, J., Fellows, C. E., and Flaud, P. M.: The visible absorption spectrum of NO3 measured by high-resolution Fourier transform spectroscopy, J Geophys Res-Atmos, 108, 2003.

Osthoff, H. D., Pilling, M. J., Ravishankara, A. R., and Brown, S. S.: Temperature dependence of the NO(3) absorption cross-section above 298 K and determination of the equilibrium constant for NO(3)+NO(2) <-> N(2)O(5) at atmospherically relevant conditions, Physical Chemistry Chemical Physics, 9, 5785-5793, 2007.

530 Osthoff, H. D., Roberts, J. M., Ravishankara, A. R., Williams, E. J., Lerner, B. M., Sommariva, R., Bates, T. S., Coffman, D., Quinn, P. K., Dibb, J. E., Stark, H., Burkholder, J. B., Talukdar, R. K., Meagher, J., Fehsenfeld, F. C., and Brown, S. S.: High levels of nitryl chloride in the polluted subtropical marine boundary layer, Nat Geosci, 1, 324-328, 2008.

Ravishankara, A. R. and Mauldin, R. L.: Temperature-Dependence of the No3 Cross-Section in the 535 662-Nm Region, J Geophys Res-Atmos, 91, 8709-8712, 1986.

Richter, A., Burrows, J. P., Nuss, H., Granier, C., and Niemeier, U.: Increase in tropospheric nitrogen dioxide over China observed from space, Nature, 437, 129-132, 2005.

Sander, S. P.: Temperature-Dependence of the No3 Absorption-Spectrum, J Phys Chem-Us, 90, 4135-4142, 1986.

540 Shardanand and Rao, A. D. P.: Collision-Induced Absorption of O2 in Herzberg Continuum, J Quant Spectrosc Ra, 17, 433-439, 1977.

Slusher, D. L., Huey, L. G., Tanner, D. J., Flocke, F. M., and Roberts, J. M.: A thermal dissociation-chemical ionization mass spectrometry (TD-CIMS) technique for the simultaneous measurement of peroxyacyl nitrates and dinitrogen pentoxide, J Geophys Res-Atmos, 109, 2004.

545 Sneep, M. and Ubachs, W.: Direct measurement of the Rayleigh scattering cross section in various gases, J Quant Spectrosc Ra, 92, 293-310, 2005.

Stutz, J., Alicke, B., Ackermann, R., Geyer, A., White, A., and Williams, E.: Vertical profiles of NO3, N2O5, O-3, and NOx in the nocturnal boundary layer: 1. Observations during the Texas Air Quality Study 2000, J Geophys Res-Atmos, 109, 2004.

550 Tan, Z. F., Fuchs, H., Lu, K. D., Bohn, B., Broch, S., Dong, H.B., Gomm, S., Häseler, R., He, L. Y., Hofzumahaus, A., Holland, F., Li, X., Liu, Y., Lu, S. H., Rohrer, F., Shao, M., Wang, B. L., Wang, M., Wu, Y. S., Zeng, L. M., Zhang, Y. S., Wahner, A. and Zhang, Y. H.: Radical chemistry at a rural site (Wangdu) in the North China Plain: Observation and model calculations of OH, HO2 and RO2 radicals, Atmos Chem Phys Discuss., doi:10.5194/acp-2016-614, in review, 2016.

555 Thalman, R. and Volkamer, R.: Inherent calibration of a blue LED-CE-DOAS instrument to measure iodine oxide, glyoxal, methyl glyoxal, nitrogen dioxide, water vapour and aerosol extinction in open cavity mode, Atmos Meas Tech, 3, 1797-1814, 2010.

Thornton, J. A., Kercher, J. P., Riedel, T. P., Wagner, N. L., Cozic, J., Holloway, J. S., Dube, W. P., Wolfe, G. M., Quinn, P. K., Middlebrook, A. M., Alexander, B., and Brown, S. S.: A large atomic chlorine source 560 inferred from mid-continental reactive nitrogen chemistry, Nature, 464, 271-274, 2010.

Varma, R. M., Venables, D. S., Ruth, A. A., Heitmann, U., Schlosser, E., and Dixneuf, S.: Long optical cavities for open-path monitoring of atmospheric trace gases and aerosol extinction, Appl Optics, 48, B159-B171, 2009.

Venables, D. S., Gherman, T., Orphal, J., Wenger, J. C., and Ruth, A. A.: High sensitivity in situ 565 monitoring of NO3 in an atmospheric simulation chamber using incoherent broadband cavity-enhanced absorption spectroscopy, Environ Sci Technol, 40, 6758-6763, 2006.

Wang, D., Hu, R. Z., Xie, P. H., Liu, J. G., Liu, W. Q., Qin, M., Ling, L. Y., Zeng, Y., Chen, H., Xing, X. B., Zhu, G. L., Wu, J., Duan, J., Lu, X., and Shen, L. L.: Diode laser cavity ring-down spectroscopy for in situ measurement of NO3 radical in ambient air, J Quant Spectrosc Ra, 166, 23-29, 2015.

Wang, H. C., Chen, J, and Lu, K. D.: Measurement of NO3 and N2O5 in the Troposphere, Prog Chem, 27, 963-976, 2015.

Wang, T., Ding, A. J., Gao, J., and Wu, W. S.: Strong ozone production in urban plumes from Beijing, China, Geophys Res Lett, 33, 2006.

Wang, T., Tham, Y. J., Xue, L. K., Li, Q. Y., Zha, Q. Z., Wang, Z., Poon, S. C. N., Dube, W. P., Blake, D. R., Louie, P. K. K., Luk, C. W. Y., Tsui, W., and Brown, S. S.: Observations of nitryl chloride and modeling its source and effect on ozone in the planetary boundary layer of southern China, J Geophys Res-Atmos, 121, 2476-2489, 2016.

Wang, X., Wang, T., Yan, C., Tham, Y. J., Xue, L., Xu, Z., and Zha, Q.: Large daytime signals of N2O5 and NO3 inferred at 62 amu in a TD-CIMS: chemical interference or a real atmospheric phenomenon?, Atmos Meas Tech, 7, 1-12, 2014.

Wangberg, I., Etzkorn, T., Barnes, I., Platt, U., and Becker, K. H.: Absolute determination of the temperature behavior of the NO2+NO3+(M)<->N2O5+(M) equilibrium, Journal of Physical Chemistry A, 101, 9694-9698, 1997.

Washenfelder, R. A., Attwood, A. R., Flores, J. M., Zarzana, K. J., Rudich, Y., and Brown, S. S.: Broadband cavity-enhanced absorption spectroscopy in the ultraviolet spectral region for measurements of nitrogen dioxide and formaldehyde, Atmos Meas Tech, 9, 41-52, 2016.

Washenfelder, R. A., Flores, J. M., Brock, C. A., Brown, S. S., and Rudich, Y.: Broadband measurements of aerosol extinction in the ultraviolet spectral region, Atmos Meas Tech, 6, 861-877, 2013.

Washenfelder, R. A., Langford, A. O., Fuchs, H., and Brown, S. S.: Measurement of glyoxal using an incoherent broadband cavity enhanced absorption spectrometer, Atmos Chem Phys, 8, 7779-7793, 2008.

Yokelson, R. J., Burkholder, J. B., Fox, R. W., Talukdar, R. K., and Ravishankara, A. R.: Temperature-Dependence of the No3 Absorption-Spectrum, J Phys Chem-Us, 98, 13144-13150, 1994.

Atmos. Meas. Tech. Discuss., doi:10.5194/amt-2016-319, 2016
Manuscript under review for journal Atmos. Meas. Tech.
Published: 10 October 2016

Atmospheric Measurement Techniques Discussions

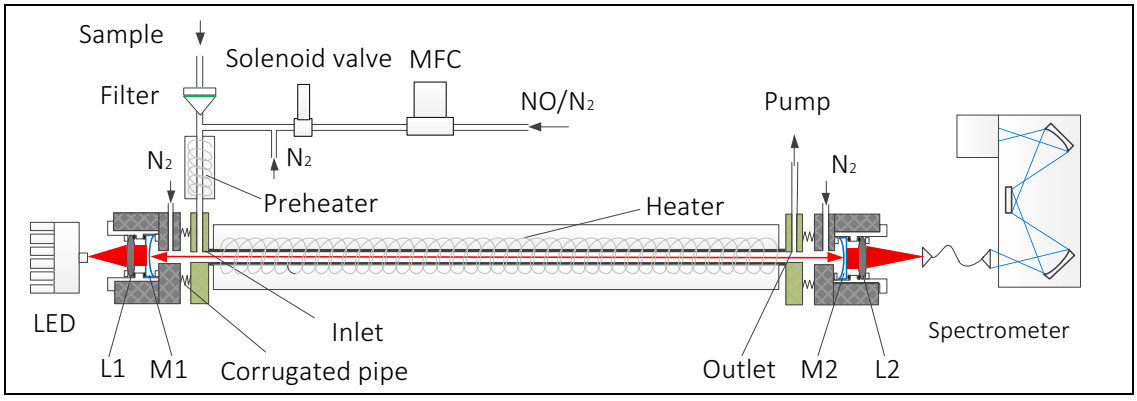

Figure.1 The schematic layout of the CEAS instrument, the optical system and the flow system are included.

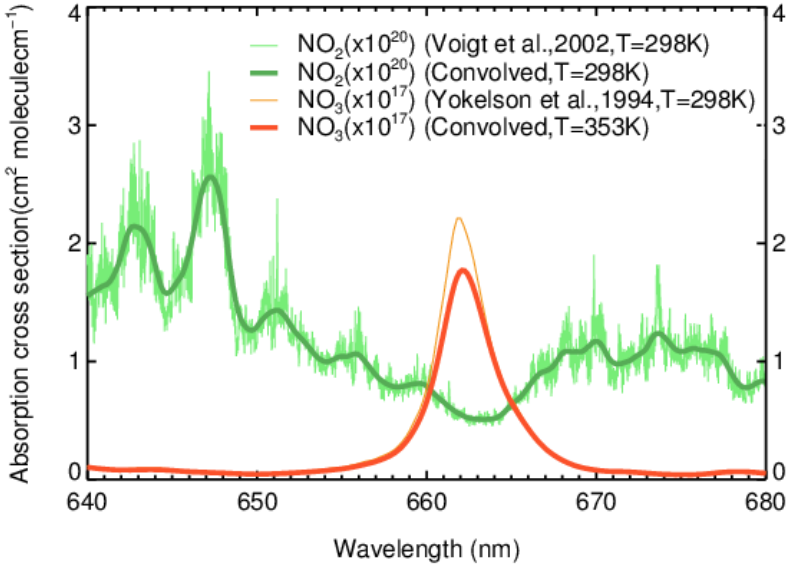

595

Figure.2 Absorption cross section of NO_3 and NO_2 from 640 to 680 nm. The green thin line is the original cross section of NO_2 at 298 K determined by Voigt et al. (2002), the green thick line is the convolved result; the orange thin line is the original cross section of NO_3 at 298 K and the red thick line is the scaled and convolved cross section at 353 K.

Atmos. Meas. Tech. Discuss., doi:10.5194/amt-2016-319, 2016
Manuscript under review for journal Atmos. Meas. Tech.
Published: 10 October 2016

Atmospheric Measurement Techniques Discussions

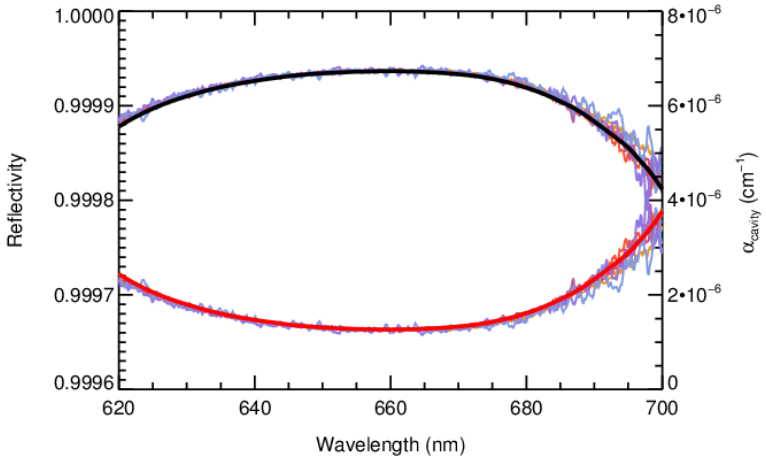

600

Figure.3 Mirror reflectivity and the cavity loss calibrated with He/N2 measurement in current experimental setup during the UCAS campaign. The original He/N_2 measurements during the UCAS campaign were depicted by varying colored lines, the smoothed black bold line is the averaged $R(\lambda)$ and the smoothed bold red line is averaged cavity loss $(1 - R(\lambda))/d$) from five measurements. The mean (±1σ) value at 662 nm of reflectivity and the cavity loss is 0.999936 ± 0.000002 and (3.534 ± 0.016) × 10^{-6}, respectively, the effective path length

605 at 662 nm reached 6.13 km.

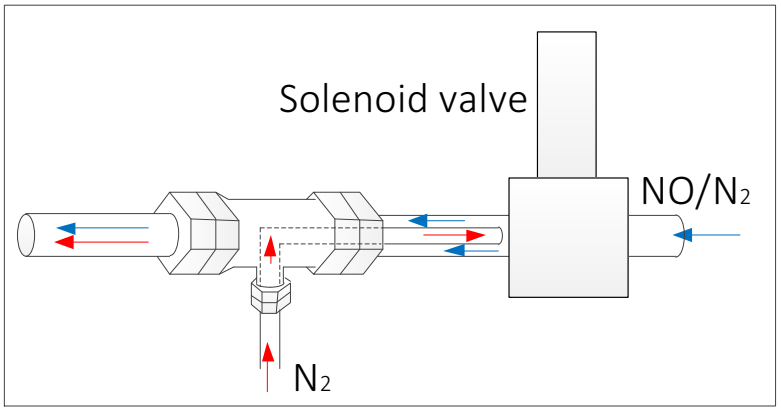

Figure.4 The schematic layout of the NO addition module, the red arrow denote the N_2 gas flow and the blue arrow denote NO gas flow.

Atmos. Meas. Tech. Discuss., doi:10.5194/amt-2016-319, 2016
Manuscript under review for journal Atmos. Meas. Tech.
Published: 10 October 2016

Atmospheric Measurement Techniques Discussions

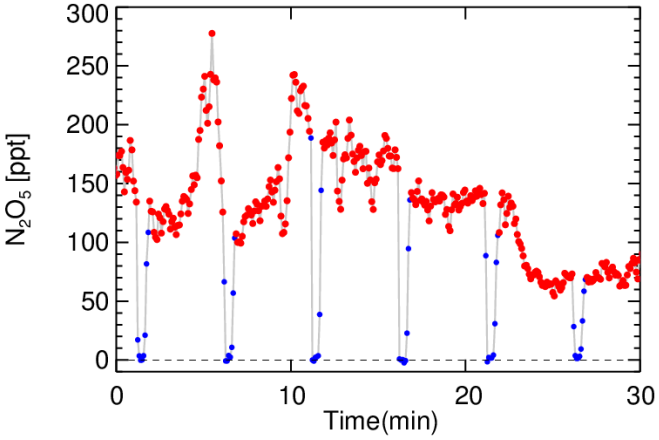

610 **Figure.5** Example time series of ambient N_2O_5 detection performed at a rural site in Beijing in 5s spectrum integral time. The red points denote the ambient measurements without addition, the blue points denote the 20 s reference measurements without addition NO and 20 s transition period measurement without addition NO.

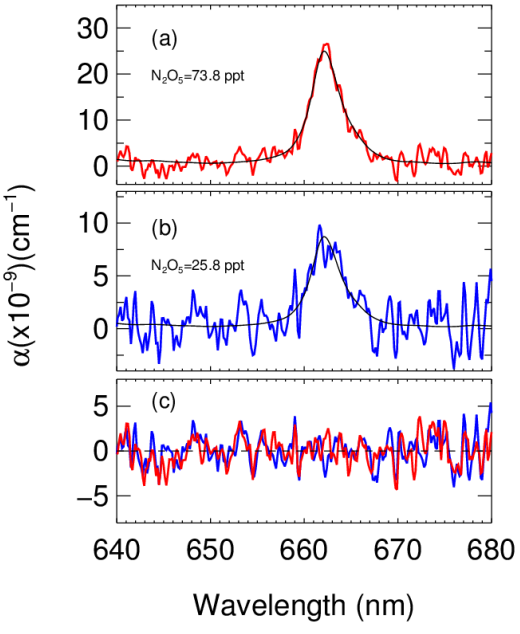

615 **Figure.6** Example of spectral fit of NO_3 radical in the heated cavity of the instrument for two ambient extinction spectrums measured in the ambient environment.

Atmos. Meas. Tech. Discuss., doi:10.5194/amt-2016-319, 2016
Manuscript under review for journal Atmos. Meas. Tech.
Published: 10 October 2016

Atmospheric Measurement Techniques Discussions

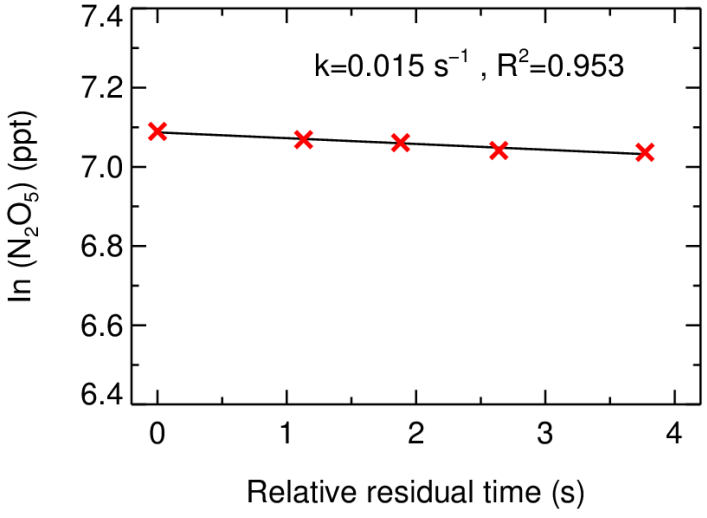

Figure. 7 The decay rate of N_2O_5 in the PFA tubes. Red points denote the observation results and the black line depicts the corresponding fit. The net wall loss reactivity of N_2O_5 is retrieved to be 0.019 ± 0.004 s^{-1} with a box model taking into account of the chemical equilibrium and purge flow dilution effect.

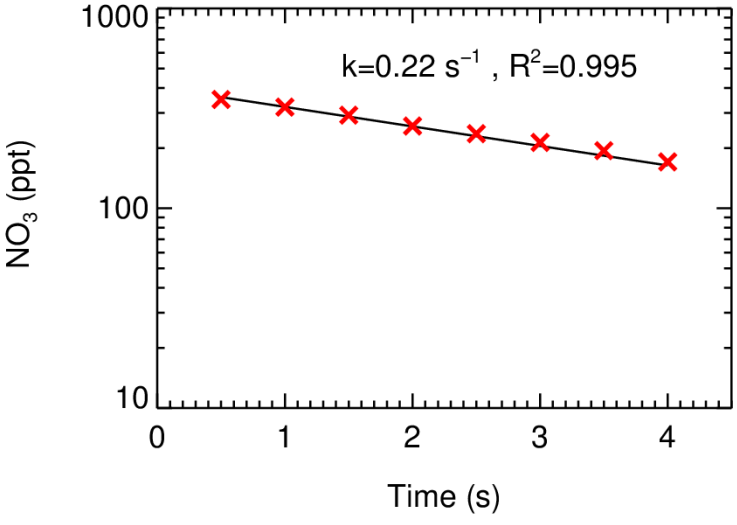

Figure. 8 The decay rate of the NO_3 radical in the heated optical cavity. Red points denote the observation results and the black line depicts the corresponding fit. The net wall loss reactivity of NO_3 is retrieved to be 0.16 ± 0.04 s-1 with a box model taking into account of the chemical equilibrium and purge flow dilution effect.

Atmos. Meas. Tech. Discuss., doi:10.5194/amt-2016-319, 2016
Manuscript under review for journal Atmos. Meas. Tech.
Published: 10 October 2016

Atmospheric Measurement Techniques Discussions

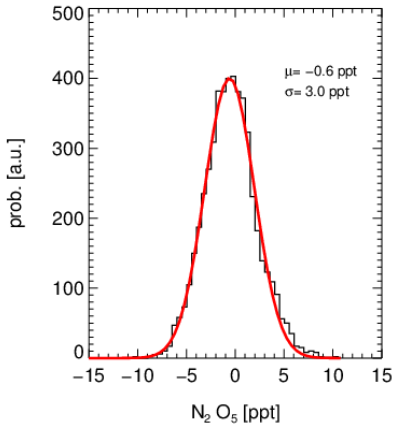

Figure. 9 The histogram of 5200 zero measurement results in the laboratory, the mean values is -0.6 ppt with the limit of detection of 3.0 ppt (1σ) with 1 second time resolution.

630

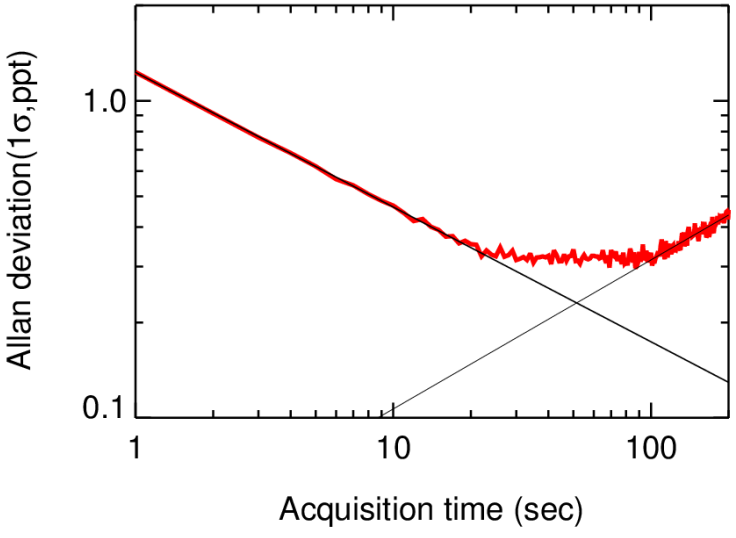

Figure. 10 Allan deviation plots for measurements of N_2O_5. 12000 zero spectrums was measured in the laboratory with 1s integration time. The best limit of the detection of this instrument is 2.1 ppt in the integral time of 50 s.

Atmos. Meas. Tech. Discuss., doi:10.5194/amt-2016-319, 2016
Manuscript under review for journal Atmos. Meas. Tech.
Published: 10 October 2016

Atmospheric Measurement Techniques Discussions

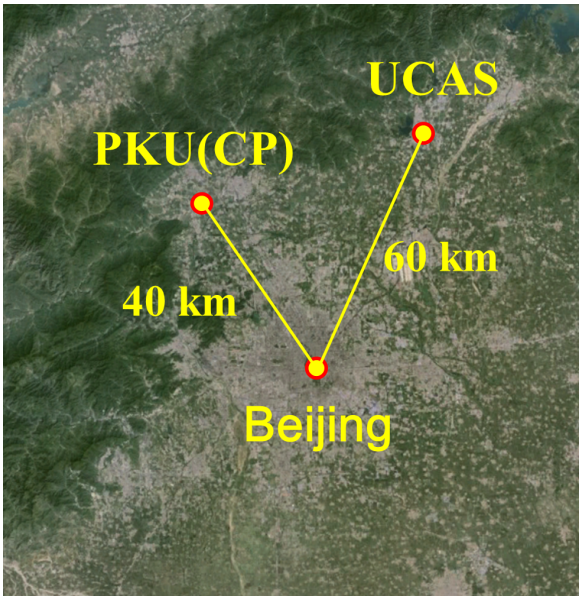

Figure.11 Map of the UCAS winter campaign 2016, the UCAS site and PKU (CP) site is about 60 km and 40 km far from the center of Beijing, respectively.

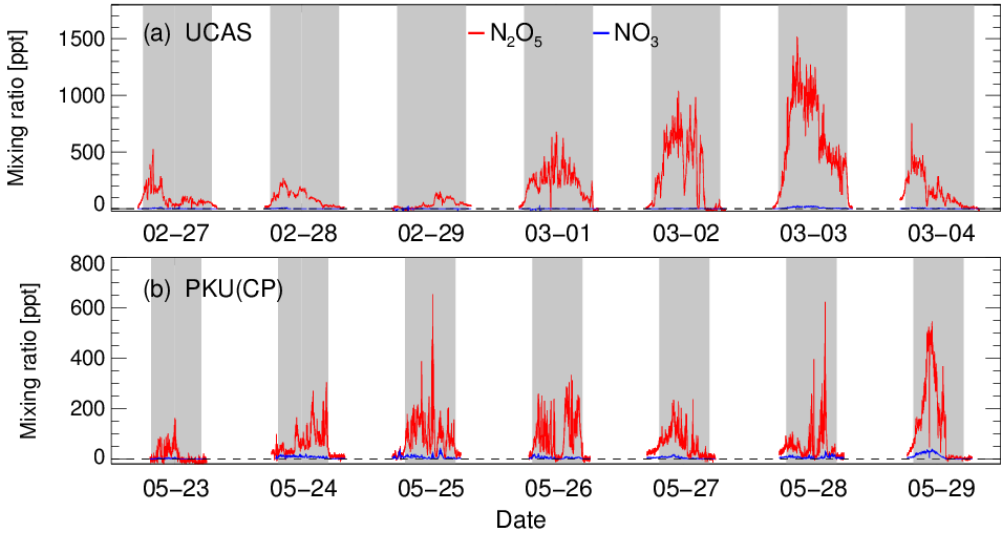

Figure.12 An example of time series of N_2O_5 during the UCAS winter campaign 2016 and the PKU (CP) spring campaign, the red line denoted N_2O_5 and the blue line denoted the calculated NO_3 based on steady state calculations, all the data was averaged to 1 minute. Panel (a) shows a typical development of the observed N_2O_5 concentrations from clean to polluted air masses from 26 February to 4 March 2016 at UCAS, panel (b) shows a typical pollution episode characterized during the PKU (CP) observations from 22 May to 29 May 2016.